Towards Predicting Radial Inflow Turbine Performance Operating with Ideal and Real Working Fluids

Fuhaid Alshammari [a], Apostolos Karvountzis-Kontakiotis [a,b] *, Apostolos Pesiridis [a], Panagiotis Giannakakis [c]

[a] Brunel University London, Department of Mechanical, Aerospace & Civil Engineering, Centre of Advanced Powertrain and Fuels (CAPF), Uxbridge UB8 3PH, UK

b City University London, School of Mathematics, Computer Science and Engineering, Northampton Square, London EC1V 0HB, UK

c Safran S.A., Magny-Les-Hameaux, 78772, France

* Corresponding author e-mail: a.karvountzis@brunel.ac.uk

Abstract

This paper outlines a novel meanline off-design model to predict the performance characteristics of a radial inflow turbine that operates with ideal and real working fluids. Experimental data available in open literature were used for validation, including radial turbines that operate with both ideal gas (air) and real working fluids (R123). Initially the differences in the expansion process between ideal and real fluids on a thermodynamic base are highlighted. Then, the proposed meanline off-design model is calibrated for a few selected points and validated against experimental data for both air and R123. The comparison between the predicted and measured results presented errors less than 10% for both ideal and real gas fluids. Finally, the predicted air turbine was simulated with a real gas fluid. Relative to air, operation with R123 revealed that the peak efficiency is 12% lower and occurs at 70% lower rotational speed. The proposed methodology gives insights for accurate model-based design of organic Rankine cycle (ORC) systems, as the radial turbo expander is the most crucial and expensive component of such heat recovery systems.

Highlights

- Presentation of a novel off-design method to predict radial inflow turbine performance
- Effect of employed working fluids on radial inflow turbine performance
- Proposed method combines 0D modeling with low computational cost and high accuracy
- Demonstration of accurate prediction of expander off-design performance for various working fluids

Nomenclature

1-5	Stations shown in Figure 1	**Subscript**	
a	Speed of sound [m/s]	b	back face
A	Area	c	corrected
b	blade height [m]	hyd	hydraulic
BK	Blockage factor [-]	opt	optimum
C	Absolute velocity [m/s]	r	radial, rotor
Cf	Friction factor [-]	rms	root mean square
Cm	Meridional velocity [m/s]	s	insentropic, stator
C_θ	Tangential velocity [m/s]	t	tip, total
Ca	Axial coefficient [-]	vol	volute
Cr	Radial coefficient [-]	x	axial
d	diameter [m]		
h	Enthalpy [kJ/kg]	Greek	
Ka	Discharge coefficient of the axial component [-]	μ	Viscosity [Pa.s]
Kr	Discharge coefficient of the radial component [-]	η	Efficiency [-]
Ka,r	Cross coupling coefficient of the axial and radial components [-]	β	Relative angle [deg]
l	length [m]	δ	Deviation angle [deg]
M	Mach number [-]	ε	Clearance [m]
$\dot{m}$	Mass flowrate [kg/s]	ρ	Density [kg/m3]
N	Rotational Speed [rpm]	α	Absolute flow angle [deg]
o	Throat opening [m]		
P	Pressure [kPa]		
r	radius [m]		
Re	Reynold number [-]		
s	Entropy [kJ/kg.k]		
T	Temperature [K]		
U	Tip speed [m/s]		
w	Relative velocity [m/s]		
W	work [kW]		
z	Axial length [m]		

1. Introduction

Transportation is responsible for about one third of global CO_2 emissions [1], while road transportation accounts for the great majority of energy consumption (~85%) and consequently the majority of greenhouse emissions [2]. Improving the thermal efficiency of internal combustion engines by reducing the waste heat losses such as heat transfer, exhaust waste heat and pumping losses are the main topics of current research.

Radial inflow turbines appear as the main tool to improve energy efficiency of automotive powertrain systems. Turbocharging, downsizing, turbocompounding and more recently organic Rankine cycles are the main applications of a radial turbine in the powertrain of a vehicle. Twin turbo, twin scroll and variable geometry turbines are some of the most popular technologies being applied in turbochargers to support engines downsizing and improve engines efficiency [3]–[6].

Considering that substantial fuel energy is dissipated in forms of heat in internal combustion engines[7], it is essential to reuse this wasted heat in order to improve fuel economy and reduce exhaust emissions. Technologies of reusing wasted heat are called waste heat recovery technologies. Lately, ORC systems gain lots of attention as a waste heat recovery technology appropriate for low to medium heat sources. This is due to the attractive combination that ORC systems can provide such as high thermal efficiency, affordability for engine exhaust WHR [8], no increase in pumping work [9], and simple and compact structure [10]. Several studies in open literature cited that applying ORC systems in ICEs is found to significantly improve the BSFC [11]–[13] and engine exhaust emissions

[14], [15]. Since they have significant effects on the overall cycle's performance and cost [16], design of an appropriate expander and selection of a suitable working fluid should receive "the lion's share" of the attention when designing an ORC system [11], [17]–[22].

Expansion machines are classified into two main types; namely, turbo-expanders and volumetric expanders. Selecting the appropriate expander strongly depends on working conditions, type of working fluid and space and weight restrictions [23]. Other factors should be considered such as power output, isentropic efficiency, lubrication requirements, reliability cost, leaking, noise and safety [24][25]. Generally, turbo-expanders are preferred when converting the extracted power to electricity while reciprocating expanders, due to their flexibility of operation, are preferred when the extracted power is coupled directly to the crankshaft [26]. Compared to turbo-expanders, volumetric expanders are usually heavier and bulkier [27]. In addition, they are used at low power outputs due to the limitation of the their rotational speeds [28] and in most applications a lubrication system is required that increases system complexity [23]. Turbo-expanders, on the contrary, are preferred due to their high power outputs and efficiencies, simpler design and the non-requirement for a lubrication system. Turbo-expanders are mainly classified into axial and radial turbines. Axial turbines are commonly used with high flow rates and low-pressure ratios. The reason for this is that, at low mass flow, the blades of an axial turbine become very small, making it difficult to maintain small tip clearance, resulting in a significant drop in efficiency [29]. Radial turbines, on the other hand, are less sensitive to blade profile [30][31] and used with high pressure ratios and low mass flow rates

[32][33] which make them practical when used in ORCs. According to Sauret and Rowlands [31], radial turbine inflow turbines are preferred over axial ones due to their robustness under increased blade loading, simpler manufacturing and improved dynamic stability. In addition, radial turbines can accommodate expansion ratio up to 9 in a single stage, while axial turbines would commonly require three stages to handle such an expansion [34].

Although the ORC system is a promising waste heat recovery technology, its cycle efficiency is low due to the low working temperature. Therefore, designing an efficient turbine and predicting its performance are of great importance to avoid further efficiency reductions. In addition, thermodynamic properties of heat sources are unstable [35][36], which makes the prediction of the turbine performance at different operating conditions even more important at the early phase of the design. In recent studies, CFD has been used extensively in predicting turbine performance as in [16], [37]–[54]. However, simulations using CFD have high computational cost and require expensive computer resources. Moreover, errors due to the finite difference approximations and the not well-known physics are common in CFD [55]. Another issue of using CFD in turbomachinery is that the accuracy of CFD is limited in highly turbulent flows [55], [56]. Therefore, predicting the off-design performance using a fast and accurate 1D model is a vital part during the design process.

The output of off-design codes is basically the characteristic curves of performance maps. These maps are then used to provide an estimate of turbine efficiency and power output at various inlet conditions and rotational speeds. In open literature, there are a number of off-design codes that are applied with air

(ideal gas) as working fluid. Jansen and Quale [57] presented a performance prediction methodology of radial turbines. Their results were in satisfactory agreement with the experiments. However, the authors stated that this methodology is preferred for pressure ratios up to 4 and under subsonic conditions. In 1968, Dadone and Pandolfi [58] conducted an off-design procedure for both small and large-size turbines. The results were in fairly good agreement with the experiments except at high expansion ratios and low equivalent speeds where a small discrepancy was noticed. NASA [59], [60] also conducted studies with off-design codes and their results were in good agreement with the experimental results. There are also other performance prediction procedures such as [61]–[64]. However, all the aforementioned methodologies are applicable when using ideal gas as the working fluid. For highly dense fluids such as organic fluids, the thermodynamic properties are different from ideal gas ones. For instance, organic fluids have high molecular weight, low boiling points and low speed of sound. Furthermore, ORC radial turbines present high expansion ratios and high Mach number at the stator exit due to the rapidly changing specific volume that results in supersonic flows.

This paper presents a novel meanline off-design model that can be employed to simulate ORC radial turbines. Once the geometry is imported, the model can accurately and with low computational cost calculate the performance curves of the expander for any real gas working fluid. Compared to air turbine models, the proposed model can contribute to the accurate simulation of the transient operation of ORC systems and utilized for the optimum selection of the working fluid. As far as the authors are aware, this is the first publicly available study

where the proposed model is validated against a real gas turbine experimental data. It is worth mentioning that this paper also highlights the differences on the expansion process when working fluid switches from ideal (air) to real gas (R123) for the same expander geometry.

2. Meanline Off-Design Model

The modeled stations and components are depicted in Figure 1. A single stage turbine consists of three main components: the volute, the stator and the rotor. The flow first enters the volute and gets accelerated and distributed uniformly around the periphery of the turbine. Moreover, the tangential component of the velocity increases before entering the nozzle vanes due to the reduced cross-section area, and flow is distributed evenly around the periphery of the stator inlet. After leaving the volute, the flow enters the stator vane where the fluid is further expanded and turned to enter the rotor blades in the optimum direction with the necessary tangential velocity. Finally, the fluid enters the most critical component of turbine, the rotor, where the fluid is further expanded converting the kinetic energy into shaft power.

The proposed model is based on the assumption that the fluid properties are constant on a plane normal to its direction of motion and thus vary only in one direction that follows the geometry of blades on the mean streamline, Figure 1. At each station, the continuity equation is used as the control point where convergence should be achieved. Moreover, a detailed losses model from open literature is applied to investigate the real turbine performance. It has to be mentioned that the presented losses submodels have been validated against air

data and their applicability on real gas conditions has not been validated by other studies. However, in this study these losses submodels are utilized and calibrated against real gas experimental data for subsonic conditions. Further research on losses mechanism is performed in parallel by City University of London [65] (EPRSRC Grant number EP/P009131/1).

The model starts by importing the turbine geometry and the thermodynamic conditions of the working fluid at the stage inlet. In addition, the optimal relative flow angle, $\beta_{4,opt}$ and deviation angle of stator α_s are considered as modelling parameters with specified default values as outlined in the next sections. Figure 2 briefly outlines the flow charts of the methodology. The modeling of each component is detailed in the next sections.

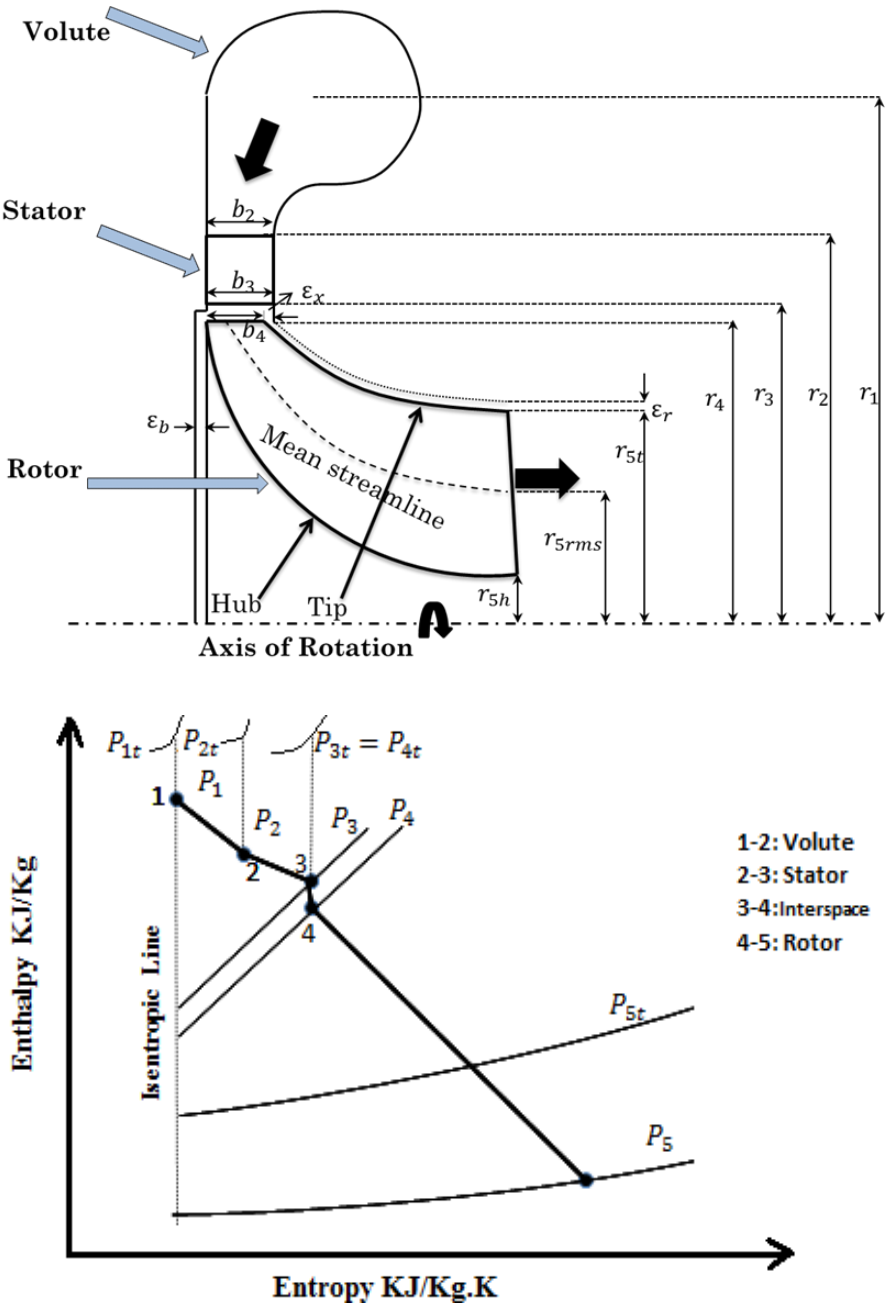

Figure 1: a) Meridional view of the turbine stage; and b) h-S expansion diagram.

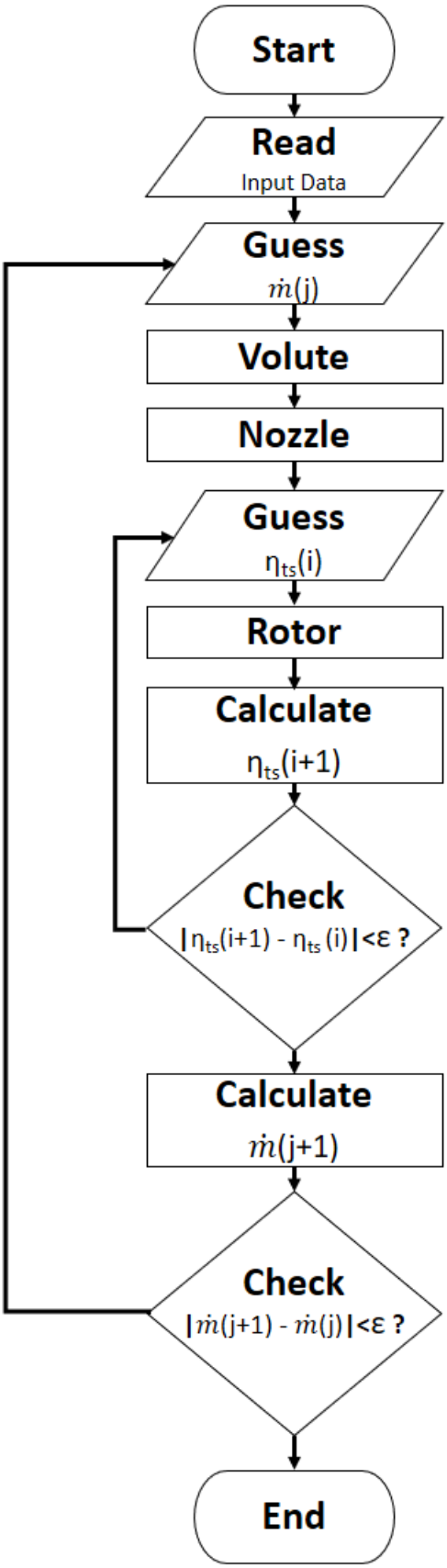

Figure 2: Flowchart of the proposed meanline off-design model for unchocked conditions.

2.1 Volute Model

At volute inlet, the absolute velocity C_1 is given an initial value. Static enthalpy is then calculated using the definition of total enthalpy, equation (1). The other thermodynamic properties are subsequently calculated using the EoS, equation (2). The process is repeated until convergence is achieved in equation (3).

$$h_1 = h_{01} - \frac{C_1^2}{2} \tag{1}$$

$$\{h_1, s_1 = s_{01}\} = EoS\ (\rho_1, T_1, a_1, P_1, fluid) \tag{2}$$

$$C_1 = \frac{\dot{m}}{\rho_1 A_1} \tag{3}$$

2.2 Stator Model

In order to calculate the velocity triangle at the stator inlet, an iterative process is required to calculate the absolute velocity C_2 until convergence is achieved for mass balance equation ($\dot{m}$). The volute losses are calculated using equation (4) [66]. Consequently, the isentropic static enthalpy h_{2s} is calculated, using equation (5), to obtain the rest of the thermodynamic properties at stator inlet as shown in equation (6) and equation (7). The new mass flow rate is then calculated as shown in equation (8) and validated with the mass flowrate assumption.

$$\Delta h_{vol} = \frac{1}{2} k_{vol} C_2^2 \tag{4}$$

$$h_{2s} = h_2 - \Delta h_{vol} \tag{5}$$

$$\{h_{2s}, S_1\} = EoS\ (P_2, fluid) \tag{6}$$

$$\{h_2, P_2\} = EoS\ (\rho_2, T_2, a_2, s_2, fluid) \tag{7}$$

$$\dot{m}_{calc} = \rho_2 A_2 C_2 \tag{8}$$

Similar to the stator inlet, stator outlet is resolved in an iterative manner until convergence of the mass flow rate is achieved, equation **(9)**. However, C_{m3} is not yet known. Initially the absolute velocity C_3 and the static entropy s_3 at stator exit are assumed. Then, the static enthalpy is calculated using the definition of total enthalpy. The other thermodynamic properties are then obtained using the EoS as shown in equation **(10)**.

$$\dot{m}_{calc} = 2\pi r_3 \rho_3 b_3 C_{m3} \tag{9}$$

$$\{h_3, s_3\} = EoS\ (\rho_3, T_3, a_3, P_3, fluid) \tag{10}$$

Continuing the above process, Baines [67] proposed a correlation to calculate the absolute flow angle at stator exit α_3, equation **(11)**. The coefficients a_0, a_1, a_2 are 6, 0.96 and -3.4, respectively [67], and δ_s is the stator deviation angle and it's a calibration parameter. Then, the other velocity components are calculated using the velocity tringle at stator outlet.

$$\begin{cases} \alpha_3 = a_0 + a_1 cos^{-1}\left(\dfrac{o_3}{s_v}\right) + \delta_s & for\ M_3 > 0.3 \\ \alpha_3 = a_0 + a_1 cos^{-1}\left(\dfrac{o_3}{s_v}\right) + a_2(Ma_3 - 0.3) + \delta_s & for\ M_3 \leq 0.3 \end{cases} \tag{11}$$

In order to validate the first assumption of s_3, the loss model at the stator outlet is applied. There are several stator loss models in the open literature such as [68]–[72]. It is worth mentioning that all these available loss models are either assessed empirically, or approximated by means of flat plate and pipe flow fiction relations

[61]. Since the loss models in this study are expressed in terms of enthalpy drop, the stator loss model proposed by Balje [72] is applied, equation **(12)**.

$$\Delta h_{stator} = 4C_f \left(\frac{l_{hyd}}{d_{hyd}}\right)\left(\frac{C_2 + C_3}{2}\right)^2 \qquad (12)$$

where C_f is the coefficient of friction in the nozzle row. Churchill [73], [74] developed a correlation of the coefficient of friction using the Moody diagram as can be seen in equation **(13)**. Re is the average of Reynolds number between nozzle inlet and exit and expressed in equation **(14)**.

$$C_f = \left[\left(\frac{8}{\overline{Re}}\right)^2 + \left(\left[2.457\, ln\left(\frac{1}{\left[7\frac{1}{\overline{Re}}\right]^{0.9} + 0.27wr}\right)\right]^{16}\left(\frac{37530}{\overline{Re}}\right)^{16}\right)^{-\frac{3}{2}} + \right]^{\frac{1}{12}} \qquad (13)$$

$$\overline{Re}_{nozzle} = \frac{\frac{C_2 b_2 \rho_2}{\mu_2} + \frac{C_3 b_3 \rho_3}{\mu_3}}{2} \qquad (14)$$

where wr is the relative wall roughness and a value of 0.0002 m was used as suggested by Aungier [75]. Once the stator loss is calculated, the isentropic enthalpy is then calculated as was shown in the volute loss model.

In ORC turbines, supersonic operation ($M_3 > 1$) is expected at the stator exit due to the higher pressure ratio of the cycle and the low speed of sound for organic fluids. For $M_3 > 1$, the flow is choked and the corrected mass flow remains constant for any pressure ratio equal or greater than the choked value. In this case, the pressure ratio can have infinite number of values at the same mass flow rate. When the blade raw is choked at the stator exit, the choked mass flow is kept fixed. Then, the velocity triangle is solved using the choking mass flow rate value without the need for iteration.

2.3 Interspace Modelling

A small space between the stator trailing edge and rotor leading edge is essential for the nozzle wakes to mix out before entering the rotor. Increasing the interspace distance will result in higher fluid friction and boundary layer growth whereas reducing the interspace distance will result in lower blade row interaction [66]. In his CFD analysis, White [76] stated that the reduction of the total pressure from the stator trailing edge and rotor leading edge is 1.45% which is sufficiently small to justify a constant total pressure in the interspace. According to Li et al.[77], the conservation of angular momentum, equation **(15)**, can be applied in the vanless space since the swirl coefficient between stator exit and rotor inlet is close to unity. Therefore, the tangential velocity at the rotor inlet $C_{\theta 4}$ can be obtained.

$$C_{\theta 3}\, r_3 \;=\; C_{\theta 4}\, r_4 \qquad (15)$$

2.4 Rotor Modelling

The rotor is the most significant component in the turbine stage since the work transfer occurs in this region. The rotor is divided into two regions; namely: inlet and outlet. In the inlet region, the flow is in the radial direction, and axial direction at the outlet. The tangential component of the velocity $C_{\theta 4}$ at the rotor leading edge has been calculated using equations **(15)**. After that, the meridional velocity C_{m4} is calculated in an iterative manner with a first assumption of $C_{m4} = C_{m3}$. The rest of the velocity parameters are calculated using the velocity triangle as shown in Figure 3. Since $s_4 = s_3$ and h_4 is found from the energy balance, the

other thermodynamic properties are found using the EoS. The process continues until convergence is achieved in equation **(16)**.

$$\dot{m}_{calc} = 2\pi r_4 \rho_4 b_4 C_{m4} \qquad (16)$$

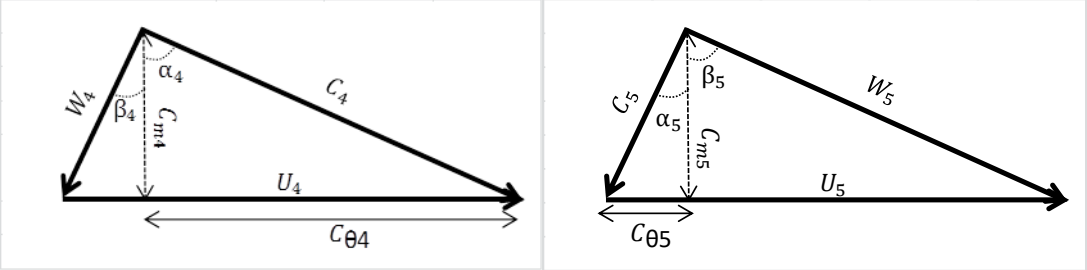

Figure 3: Velocity Triangles at Inlet (left) and Exit (right) of Rotor Blades

The prediction of the velocity triangle, Figure 3, and the thermodynamic properties at the rotor exit are not straight forward. Although the rotor exit tangential velocity $C_{\theta 5}$ is usually assumed zero at the design point, it is calculated at the off-design process for more accurate results using the Euler equation, equation **(17)**.

$$\Delta h_{act} = U_4 C_{\theta 4} - U_5 C_{\theta 5} \qquad (17)$$

The isentropic and actual enthalpies and the turbine power output are calculated using equations **(18)**, **(19)** and **(20)** respectively, after specifying an initial value for the total to static efficiency η_{ts}. Since $s_{5s} = s_{01}$, Figure 1, and the isentropic pressure at the rotor exit P_{5s} is calculated from the given pressure ratio, the isentropic enthalpy h_{5s} can be found using the EoS.

$$\Delta h_{is} = h_{01} - h_{5s} \qquad (18)$$

$$\Delta h_{act} = \eta_{ts} * \Delta h_{is} = h_{01} - h_{05} \quad (19)$$

$$W_{out} = \dot{m}\Delta h_{act} \quad (20)$$

The rotor exit velocity triangle is still incomplete. Therefore, the rotor exit relative flow angle β_5 is calculated using the equation presented in Benson [78]. Benson [78] stated that β_5 should be calculated using the cosine rule at the mean radius, while some deviation due to rotor speed may be present. Therefore, the cosine rule is applied in the current study and the rotor deviation angle δ_r is defined as shown in equation **(21)**. The velocity triangle is now complete at the rotor exit and the thermodynamic properties are subsequently obtained using the EOS.

$$\beta_5 = -\cos\left(\frac{o_{r,rms}}{s_{r,rms}}\right) + \delta_r \quad (21)$$

In order to validate the initial assumption of the total to static efficiency η_{ts}, a rotor loss model is implemented in the off-design process as shown in equation **(22)**. These losses are briefly presented here , and explained in details in [66].

$$\Delta h_{loss,rotor} = \Delta h_{incidence} + \Delta h_{passage} + \Delta h_{tip} + \Delta h_{windage} + \Delta h_{exit} \quad (22)$$

An incidence loss results from the blade loading that causes the fluid to enter the rotor at an angle that differs from the optimum one. Equation **(23)** presents the incidence loss.

$$\Delta h_{incidence} = \frac{1}{2}[W_4 \sin(\beta_4 - \beta_{4,opt})]^2 \quad (23)$$

The optimal relative flow angle $\beta_{4,opt}$ can be calculated using Stanitz correlation [79] where the centrifugal compressor slip factor is used. Therefore, it is considered as a modelling parameter in the current study.

Passage loss includes any loss within the blade passage such as secondary flow and mixing flow loss. Wasserbauer and Glassman [59] developed an expression to predict the passage loss as shown in equation **(24)**. The coefficient K is given a value of 0.3 as recommended by [59].

$$\Delta h_{passage} = 0.5\, K\, (W_4^2 cos^2 i + W_5^2) \tag{24}$$

An inevitable leakage occurs in the rotor blades from the pressure surfaces to the suction surfaces due to the gap between the turbine casing and the rotor. The minimum clearance is usually a compromise between manufacturing difficulty and aerodynamic requirements [80]. The clearance loss is calculated using equation **(25)**:

$$\Delta h_{tip} = \frac{U_4^3 Z_r}{8\pi}\left(K_a \varepsilon_a C_a + K_r \varepsilon_r C_r + K_{a,r}\sqrt{(\varepsilon_a \varepsilon_r C_a C_r)}\right) \tag{25}$$

where C_a *and* C_r are the axial and radial coefficient for the tip clearance model and they are calculated using equations **(26)** and **(27)**, respectively:

$$C_a = \frac{1 - \frac{r_{5,sh}}{r_4}}{C_{m4} b_4} \tag{26}$$

$$C_r = \left(\frac{r_{5,sh}}{r_4}\right)\frac{Z_r - b_4}{C_{m5} r_5 b_5} \tag{27}$$

Another leakage occurs between the back-face of the rotor and the housing with the air trapped in-between causing frictional losses. However, this gap generates higher centrifugal stresses than the tip clearance gaps [81]. The leakage is called windage loss and its correlation is shown in equation **(28)**.

$$\Delta h_{windage} = k_f \frac{\bar{\rho} U_4^3 r_4^2}{2\dot{m}} \tag{28}$$

where k_f denotes the empirical correlation for frictional torque by Daily and Nece [82] and has two different definitions based on the nature of the flow as follows:

$$k_f = \frac{3.7\left(\frac{\varepsilon}{r_4}\right)^{0.1}}{Re^{0.5}} \quad \text{for laminar flow } (Re < 10^5) \tag{29}$$

$$k_f = \frac{0.102\left(\frac{\varepsilon}{r_4}\right)^{0.1}}{Re^{0.2}} \quad \text{for Turbulent flow } (Re > 10^5) \tag{30}$$

Last but not least, the internal energy at the rotor exit is converted into kinetic energy and it increases with higher swirl angles. This kinetic energy is unusable and therefore considered as an additional loss. Some of the energy can be recovered by implementing a diffuser which converts a portion of this kinetic energy into static pressure. The prediction of kinetic energy loss is based on the equation **(31)** as reported in [83].

$$\Delta h_{exit} = \frac{1}{2} C_5^2 \tag{31}$$

The new efficiency is then calculated as shown in equation **(32)** and compared with the initial guess. The process is repeated until convergence is achieved.

$$\eta_{ts} = \frac{\Delta h_{act}}{\Delta h_{act} + \Delta h_{loss,volute} + \Delta h_{loss,stator} + \Delta h_{loss,rotor}} \tag{32}$$

In addition, the mass flow rate is calculated at the rotor exit using equation (33) in order to validate the first assumption at the volute inlet. If the two values don't match, a new mass flow rate is assumed and the process starts again. Although choking is unlikely at the rotor throat, similar treatment to the stator model has been added when choking takes place at the rotor.

$$\dot{m}_5 = \rho_5 C_{m5} A_5 \tag{33}$$

3. Experimental Data

In order to evaluate the reliability of the proposed off-design performance estimation methodology, the results of the proposed novel expander model are compared with two experimental works available in open literature. These cases are selected due to the sufficient geometric data available which can be implemented in the MOC, and the reliable and good quality results can be obtained.

Turbine A was tested by Spence et al. [84] with air as working fluid. The tests were conducted at a range of turbine speeds between 30,000 and 60,000 rpm, and pressure ratios between 1.3 and 4. Seven stator configurations were used in the test. All configurations have the same basic blade shape but at different blade angle and consequently a different throat area. In the current study, only one throat opening (4 mm) is evaluated.

However, it is important to also evaluate the proposed methodology using real fluids. Therefore, the model has also been used to predict the performance of Turbine B which was measured by Shao et al. [85] with the R123 (high dense

organic fluid) as working fluid and with fixed stator configuration (i.e fixed throat opening). Different heat source temperatures were investigated in [85]. The isentropic total-to-total efficiency was investigated at turbine speeds from 20,000 rpm to 54,000 rpm, and pressure ratios from 1.4 to 2.6. In the current study, a heat source of 120 C° is selected to validate the results of the model. Detailed geometry parameters for both turbines (A and B) are presented in Table 1. In addition, Table 2 presents the input thermodynamic parameters for both turbines.

Table 1: Geometrical parameters of Turbine A and Turbine B

Parameter	Symbol	Turbine A	Turbine B
Nozzle vane number	-	16	17
Nozzle inlet diameter	r_2	152.0 mm	70.0 mm
Nozzle vane height	b_2	10.2 mm	10.2 mm
Rotor inlet tip diameter	d_4	99.06 mm	99.06 mm
Rotor inlet tip width	b_4	10.2 mm	10.2 mm
Rotor inlet blade angle	$\beta_{blade,4}$	0 deg	0 deg
Rotor blade number	-	11	12
Rotor exducer tip diameter	r_{5t}	79.0 mm	34.0 mm
Rotor exducer hub diameter	r_{5h}	30.0 mm	19.0 mm
Rotor exducer blade thickness	t_5	1.6 mm	1.6 mm
Rotor exit radial clearance	ε	0.4 mm	0.4 mm

Table 2: Thermodynamic parameters of Turbine A and Turbine B

Parameter	Symbol	Turbine A	Turbine B
Inlet Stagnation Pressure [kPa]	P_{01}	141.86 – 506.63	220 - 440
Inlet Stagnation Temperature [K]	T_{01}	400	393.15
Corrected Mass Flowrate [kg/s]	$\dot{m}_c$	0.094 – 0.153	0.019 – 0.07
Pressure Ratio [-]	PR	1.3 - 5	1 - 4
Rotational Speed [RPM]	N	30,000 – 60,000	20,000 – 51,000

4. Results & Discussion

This section presents the results of the current study. Firstly, the expansion process is studied in terms of the differences between ideal and real gas EoS. Then, the proposed turbine model is validated against experimental data where the working fluid is air (Turbine A) and R123 (Turbine B). Finally, the proposed model is employed to develop a performance map for real gas R123 utilizing the geometry of Turbine A. The results are discussed and compared with air data.

4.1 Expansion Process

The majority of the off-design methodologies available in open literature describe air turbine expansion where air properties are applied. Air is modelled as an ideal gas, of which the properties are well described by the ideal gas EoS and the assumptions of constant specific heat ratio and supersonic compressibility relations are realistic. In ideal gases, the intermolecular forces are negligible in which the molecules are faced as perfectly elastic. However, the intermolecular attractive forces in real fluids such as organic fluids are non-negligible and the ideal gas assumptions introduce a significant error in the calculations.

Cubic EoS are commonly applied methods that can be utilized to model the thermo-physical properties of a real fluid at different conditions of pressures and temperatures. The equations determine the pressure of the fluid as a function of temperature and specific volume and are called cubic equations as they can be written in the form of a cubic function of molar volume. The most common EoS are the Standard Redlich Kwong (SRK), Aungier Redlich Kwong (ARK), Soave Redlich Kwong (SORK) and Peng Robinson (PR). Redlich and Kwong [86] proposed a

temperature dependence approach which improved the accuracy of the Van der Waals equation of state. Later, Soave [87] and Peng and Robinson [88] proposed additional modifications to the Redlich-Kwong [86] equations of state to more accurately predict the vapour pressure, liquid density, and equilibrium ratios. In all the above equations of state, the fluid properties such as critical point, specific volume, acentric factor and molar mass need to be specified.

REFPROP is an alternative way of calculating the thermo-physical properties of real fluids. REFPROP is a NIST computer program [89] that uses advanced equations of state which are more accurate than cubic equations of state and can provide an accurate database of the thermodynamic and transport properties. The basic properties of the R123 real fluid used in this study are presented in Table 3.

This study proposes a novel off-design method that can be used for both air expansion (Turbine A) and real fluid expansion (Turbine B). The operating conditions of real fluid expansion (R123) do not exceed an inlet pressure of 5 bar while the inlet temperature is about 400K. Figure 4 and Figure 5 illustrate relative deviations for pressure and heat capacity (Cp) respectively between ideal gas EoS and REFPROP. Within the range of thermodynamic conditions of this work, the error on pressure prediction can be up to 20% while heat capacity can be underestimated by up to 10%. Moreover both figures demostrate that at higher inlet pressure conditions the relative error for both pressure and heat capacity is increased exponentially. In fact, radial turbine expanders are operated at high pressure ratios, where errors on pressure and heat capacity can exceed 50%.

Table 3: Thermophysical properties of R123

Property	**Value**
Critical Temperature (T_{cr})	456.83 K
Critical Pressure (Pcr)	3.67 MPa
Critical Density (ρ_{cr})	3596.4 mol/m^3
Boiling Point	288.3 K
Molecular Mass (w)	152.93 g/kmol
Global Warming Potential (GWP)	77

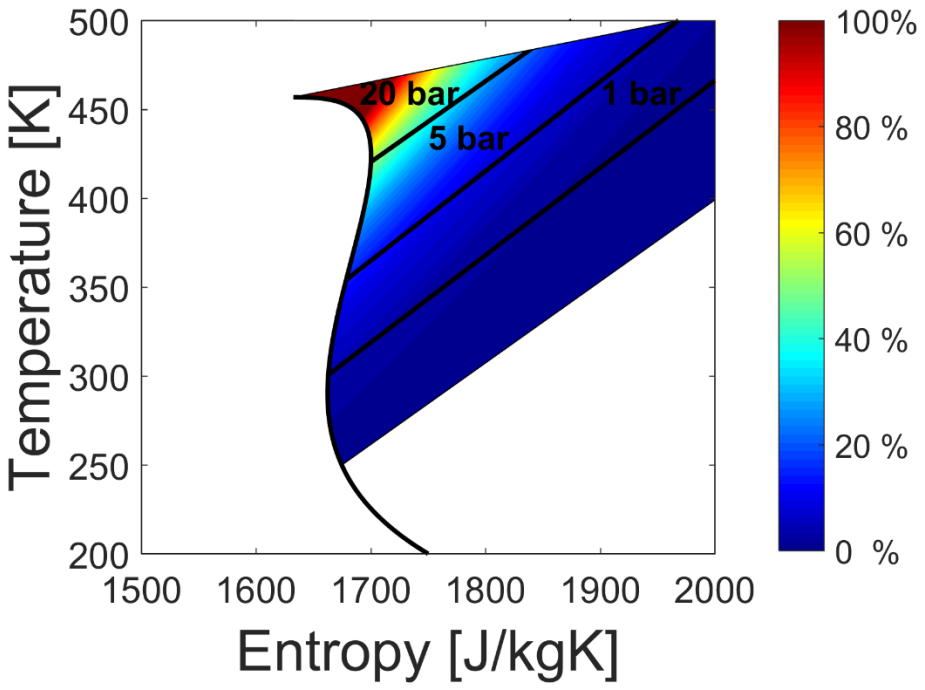

Figure 4: Pressure deviation of R123 between ideal gas EoS and REFPROP.

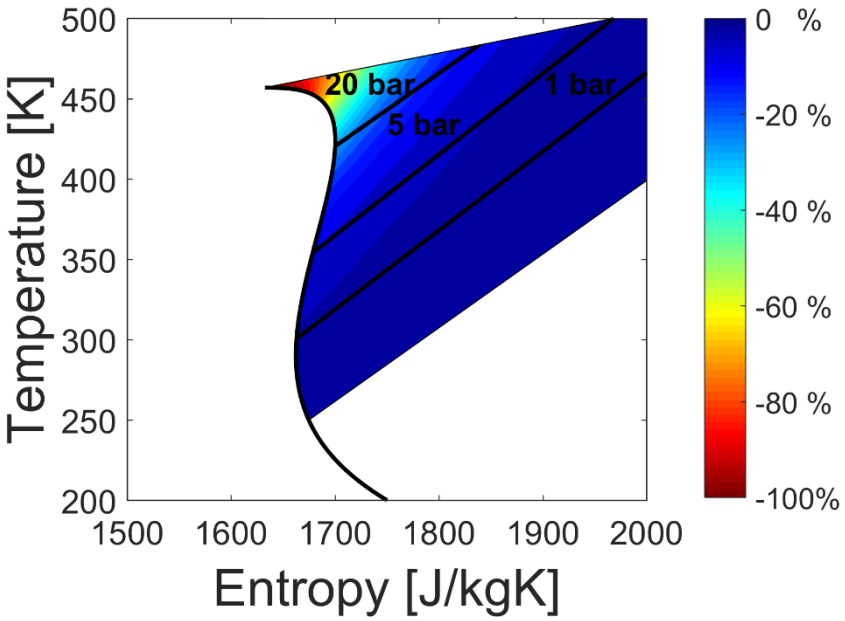

Figure 5: Cp deviation for R123 between ideal gas EoS and REFPROP.

4.2 Model Validation Using Air Data

The proposed off-design model was initially validated against air experimental data (Turbine A). The model is applied to predict the entire turbine map under various mass flowrate, rotational speed and pressure ratio operating conditions. Calibration parameters are divided into parameters that are dependent on the expander geometry and can be applied on the entire turbine map and those which are dependent on rotational speed. The most important rotational speed dependent parameter was found to be the passage loss coefficient that requires one operating point at each constant speed line for calibration while the other experimental data are used for model validation. The selected calibrated values for the turbine model include the losses mechanism, the blockage factors and the parameters for the deviation angle model. The latter is calibrated to predict the turbine mass flowrate while all parameters can affect the calculated isentropic efficiency. The calibrated values are briefly described in Table 4. Lower

passage loss coefficient values were required for higher rotational speeds while at low rotational speed higher passage loss coefficient value is applied. Furthermore, Moustapha et al. [66] reported that radial inflow turbines present optimum performance when the incidence angle lies in the range of $-40^o\ to\ -20^o$. This range was found to match in this case.

Table 4: Calibration parameters of the model for the case of Turbine A.

Description	Parameter	Value
Optimum incidence angle		-20°
Stator deviation angle		-0.4°
Stator blockage factor		0.05
Rotor deviation angle		0°
Rotor blockage factor		0.05
Passage loss coefficient		0.1-0.7

Prediction of the mass flowrate was initially evaluated. Figure 6 presents the comparison between the experimental and predicted corrected mass flowrates for different rotational speeds and pressure ratio conditions. Simulation results show that the increase of rotational speed leads to higher pressure ratio for the same mass flow rate. It is also revealed that the critical mass flowrate is achieved close to 5 pressure ratio and over this critical value the turbine is choked.

The deviation between experimental and simulated values is illustrated in Figure 7. Overall, results are in good agreement with the experimental results. The maximum deviation is 9% and is observed at the 30,000 rpm speed line and low pressure ratio. As pressure ratio is increased, deviation between calculated and experimental values is decreased. This trend was found to be consistent for all speed lines, where maximum deviation values are observed at low pressure ratios.

For typical operating conditions of PR=2.5 and higher, the observed error is less than 5% for all tested rotational speeds. The latter indicates that the proposed model is appropriate to predict the off-design performance of an air turbine. Furthermore, it can also be used to extrapolate the entire turbine map or accurately interpolate data at non-measured rotational speed conditions (map interpolation).

The capability of the model to predict the total to static isentropic efficiency has been also evaluated. Figure 8 illustrates the comparison between measured and simulated total-to-static isentropic efficiency for various pressure ratios and rotational speeds. The typical crescent curve shape of isentropic efficiency is well predicted by the model, where peak values appear at higher rotational speeds as pressure ratio is increased. However it is observed that under all speed conditions and in the area of high pressure ratios where the isentropic efficiency drops, the error between the model and the experimental data is higher.

The latter observation is better demonstrated by Figure 9 which shows the isentropic efficiency deviation between simulation and experimental values. It is shown that error increases at higher pressure ratios. The explanation of this deviation can be sought in the experimental data rather than the simulation. In this experimental study it was mentioned that some unusually high values were observed at high pressure ratios and Mach numbers [84], while similar errors between experimental and simulation values where observed in previous studies [90].

Apart from the fact that at high pressure ratios experimental error is higher, the overall picture of model prediction is quite satisfactory. Average error is less than 2.8%. The minimum average error of 0.85% was observed at 60000rpm while the maximum average error of 2.7% was observed at 40000rpm Overall, the agreement between the predicted and measured values of total-to-static isentropic efficiency η_{ts} is good over the entire range of operation.

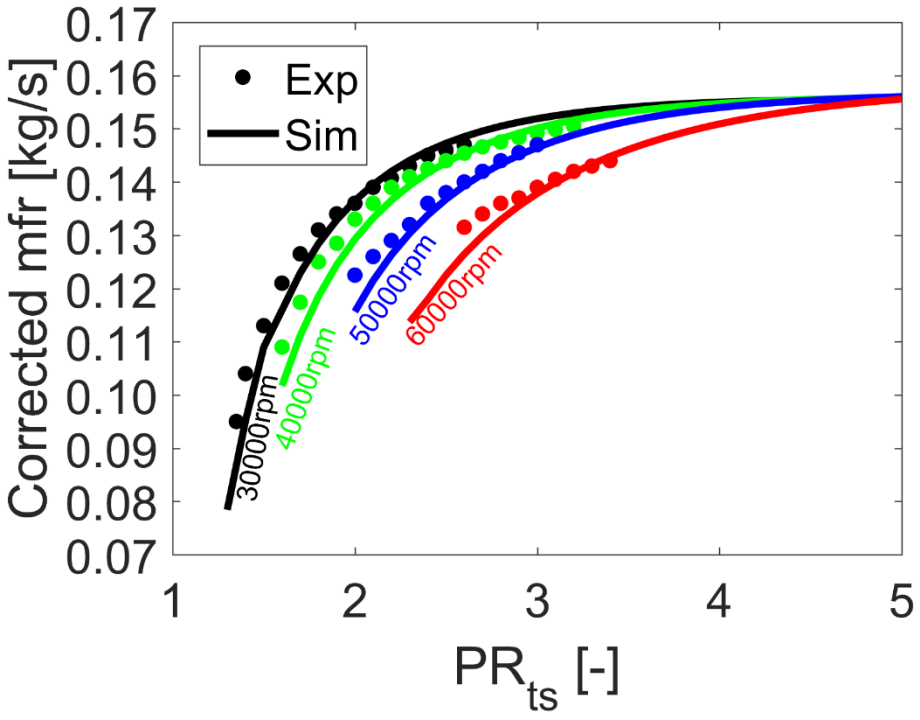

Figure 6: Comparison between the predicted and measured corrected mass flowrate for air data (Turbine A).

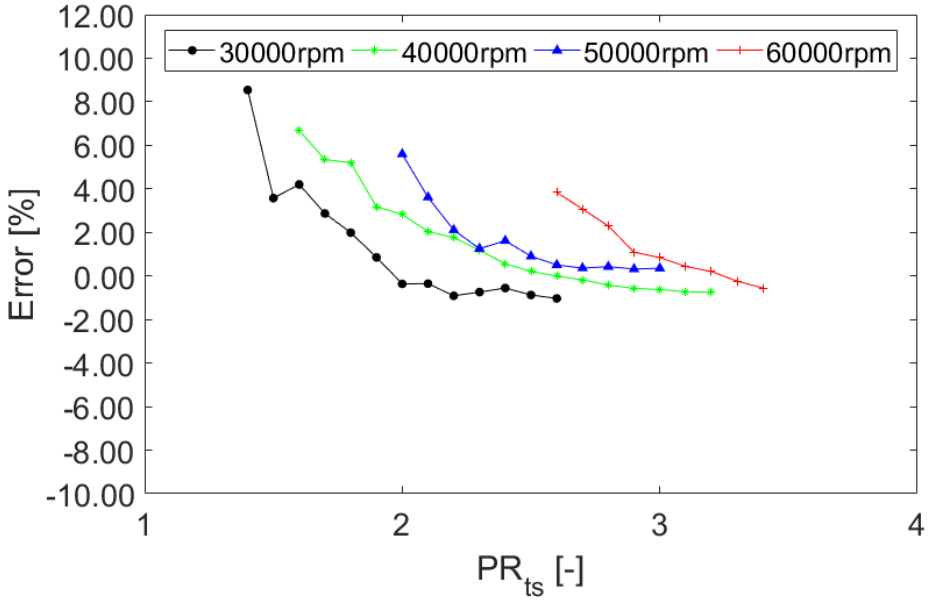

Figure 7: Deviation between predicted and measured mass flowrate for air data (Turbine A).

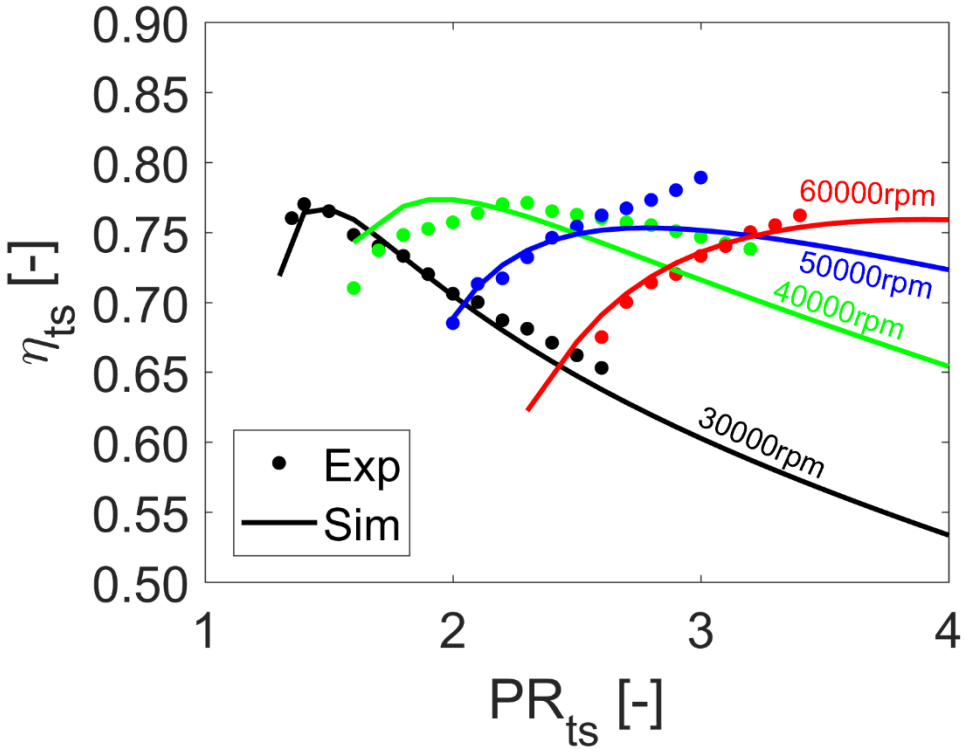

Figure 8: Comparison between the predicted and measured η_{ts} for air data (Turbine A).

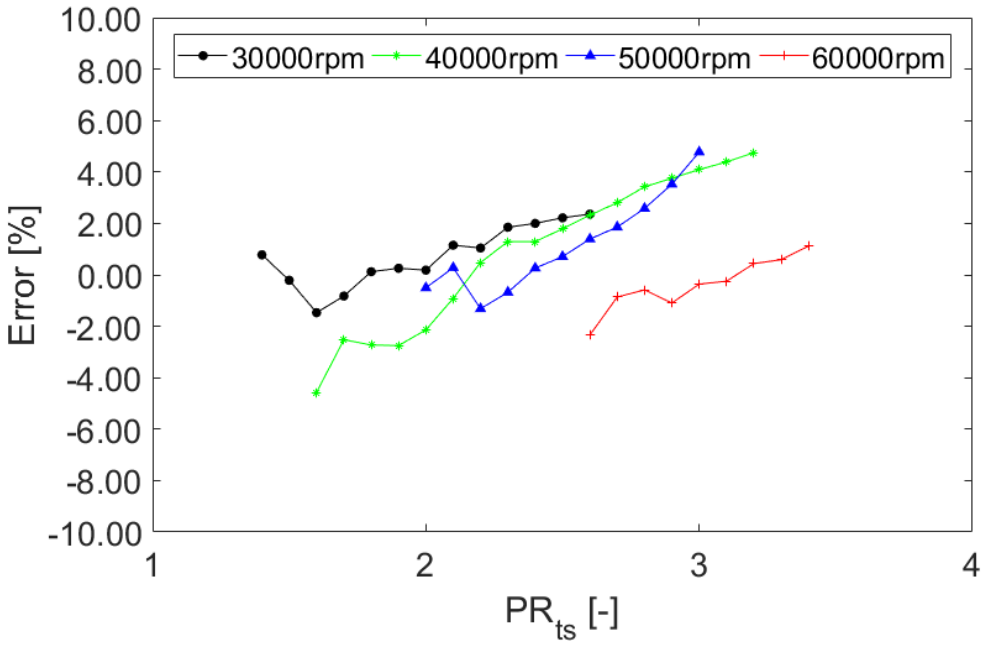

Figure 9: Deviation between predicted and measured η_{ts} for air data (Turbine A).

4.3 Model Validation Using Real Gas Data

The next step of this study is to evaluate the ability of the proposed turbine model to reproduce the performance of a radial turbine that operates with real gas. Unfortunately, detailed experimental data with real fluids are very limited in open literature. Either the expander map without the expander geometry is provided, or in most studies the expander geometry is given and accompanied only with the design point performance.

A recent study [85] presents both the expander geometry and off-design points of a radial expander operating with R123 as working fluid. In this study, the mass flowrate is not measured; instead the generator power driving the expander is plotted against rotational speed. For the validation of the model, the expander power output can be used instead of the mass flow. The expander power output has been calculated by dividing the generator power with a constant

efficiency value of 0.9 at all operating points. Total isentropic efficiency and total pressure ratio of the expander have been calculated from temperature and pressure measurements performed upstream and downstream of the expander.

The model calibration has been performed by using the air data coefficients presented in Table 4, as the R123 experimental data are not detailed. Compared to the air data (Turbine A) where the passage loss coefficient was a function of rotational speed, in this case the passage loss coefficient was tuned at a fixed value for all rotational speeds. The calibrated value is equal to 0.3 as this value minimizes the error at the peak efficiency point. The validation between the experimental data and the proposed model for both total-to-total isentropic efficiency and expander power output is shown in Figure 10 and Figure 11. Peak efficiency is predicted at 2500rpm higher than the experimental value while the typical efficiency curve is qualitatively well predicted. Furthermore, the expander power output is almost linearly increased as a function of rotational speed.

The errors between experiment and simulation for both isentropic efficiency and expander power are depicted in Figure 12. The prediction of the turbine isentropic efficiency is satisfactory over the entire range of operation. The maximum error of 6.6% is observed at 51,000 rpm followed by a 4.2% error at 44,000 rpm. A similar picture is presented for the prediction of the expander power. The predicted power output match the measured values over the entire range of rotational speed and the maximum error of 6.2% is observed at 44,000 rpm.

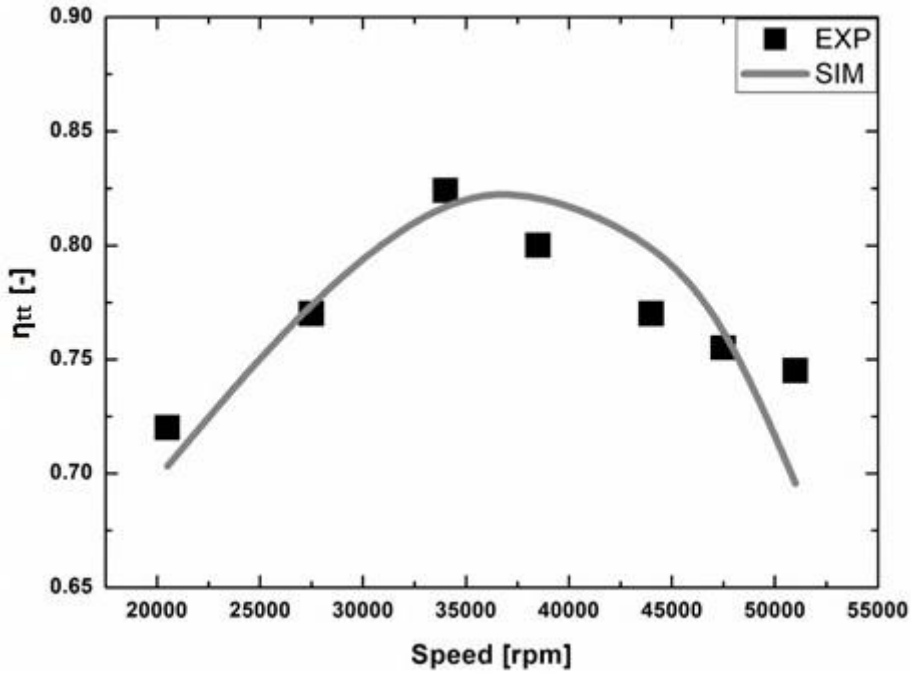

Figure 10: Comparison between the predicted and measured η_{tt} for R123 (Turbine B).

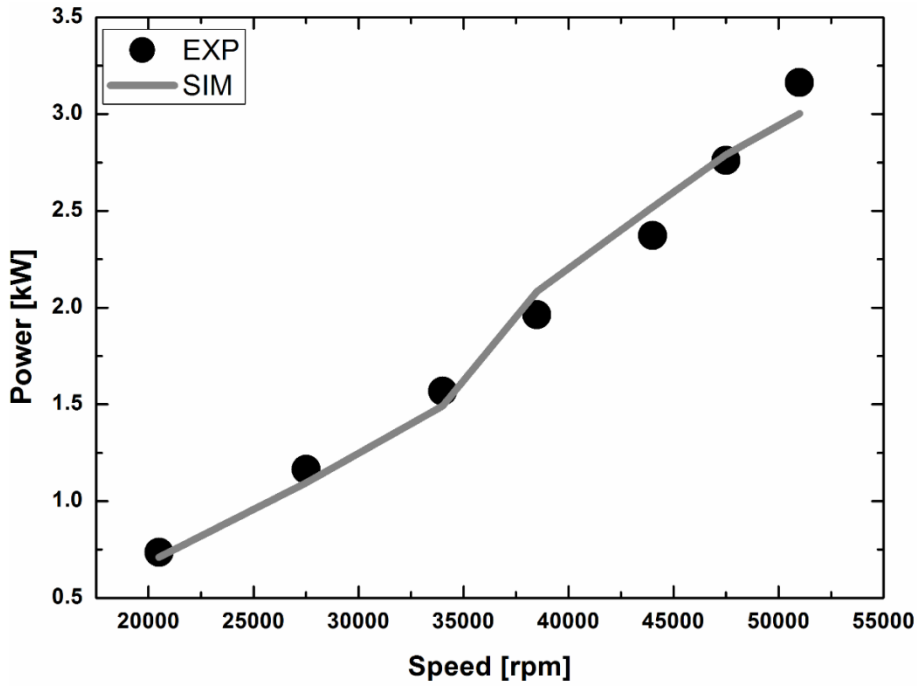

Figure 11: Comparison between the predicted and measured W_{out} for R123 (Turbine B).

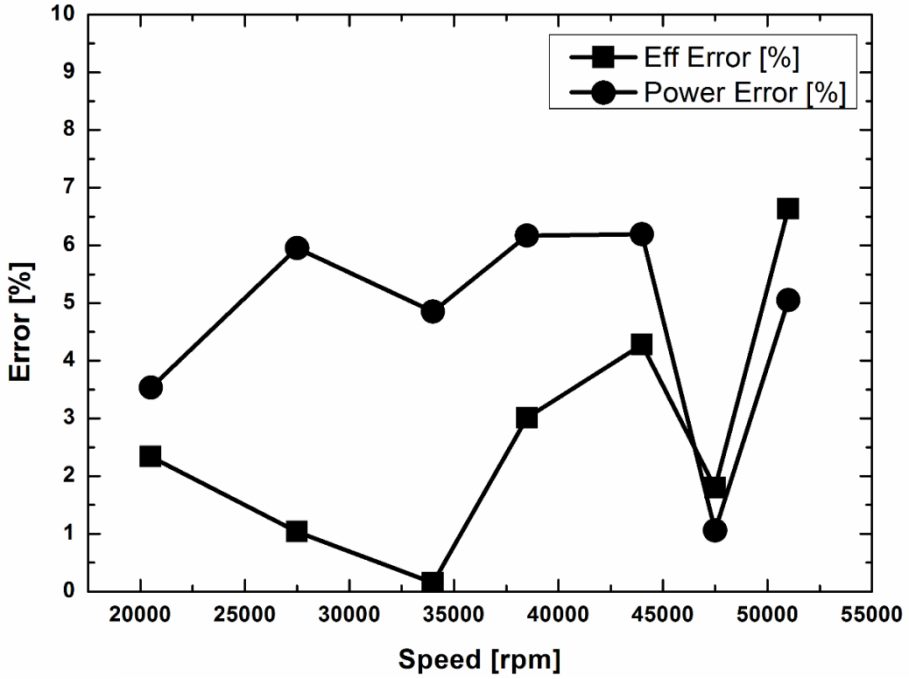

Figure 12: Deviation between predicted and measured for R123.

4.4 Effect of Real Gas on an air turbine Off-Design Map

The model validation has shown that the proposed model can efficiently calculate the off-design map of a radial expander when the geometry is known for any working fluid. The latter can be performed accurately, with low computational cost and without the need of expensive experimental tests. Tuning coefficients can further improve the accuracy of the model, when experimental data are available.

To this end, the geometry of the air turbine (Turbine A) has been utilized to predict the off-design map of when R123 is used as a working fluid. Significant differences between air and R123 such as fluid density, speed of sound and viscosity have to be considered when an air turbine is employed as a real gas expander. In a recent study, White and Sayma [91] presented an advanced similitude theory that can be employed for organic fluids under both subsonic and

supersonic conditions. Based on this study, the operating conditions of a radial expander are expected to change significantly when working fluid alters.

The off-design expander efficiency map of Turbine A that operates with R123 is illustrated in Figure 13. As experimental data are not available for this model based analysis, the calibrated coefficients of Turbine A were employed. Figure 13 shows that the maximum isentropic efficiency occurs at low rotational speed and pressure ratios, while the peak efficiency decreases for higher rotational speeds. Compared to the air turbine, real gas turbine rotational speed is approximately two (2) times lower, which is equal to the ratio of speed of sound for air and R123 [91]. For rotational speeds higher than 30000rpm, the isentropic efficiency of the expander was found poor (>0.2) and is not illustrated.

Figure 14 presents the corrected mass flowrate of Turbine A that operates with R123 as a function of pressure ratio and rotational speed. Compared to the air turbine, the corrected mass flowrate was found to be about 2.5 times higher due to the higher density of the real fluid at similar thermodynamic conditions. It is also shown that at pressure ratios higher than four (4), the expander is chocked. However it is expected that the model cannot accurately predict the performance of the radial expander that operates with real gas under supersonic conditions, as losses submodels are not valid for under those conditions, therefore the area of interest is restricted at subsonic conditions.

The prediction of the mass flowrate of a radial expander that operates with real gas fluids can be also valuable in ORC measurements. In typical organic Rankine cycle systems, the measurement of the mass flowrate of a real gas at vapour phase can be extremely expensive and therefore is omitted. The common practice is to

measure the generator power output, and calculate the mass flowrate by assuming the generator's efficiency. The latter increases the experimental error. The proposed model can be valuable as it can provide lookup tables of the mass flowrate which can run online in data processing, in order to estimate a more accurate flowrate based on temperature and pressure measurements at each time step. The proposed novel turbine model can also be applied in ORC working fluids optimization, especially for systems that operate under transient conditions, as each working fluid can lead to a unique off-design expander map.

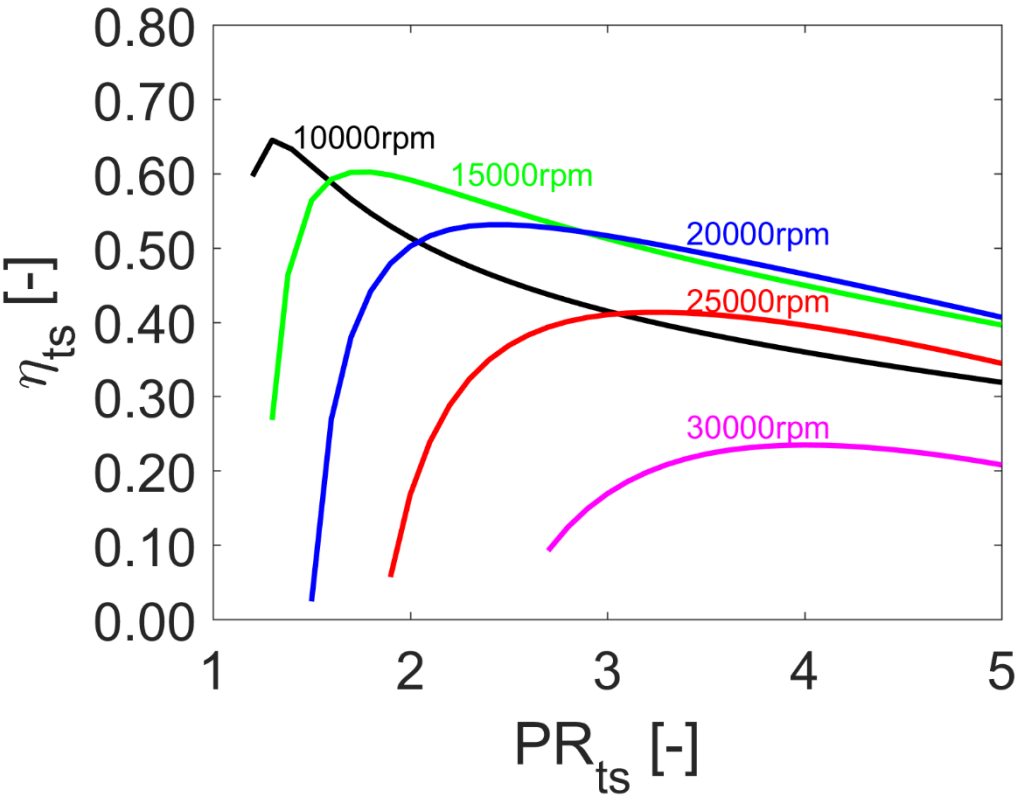

Figure 13: Prediction of efficiency map for Turbine A using R123.

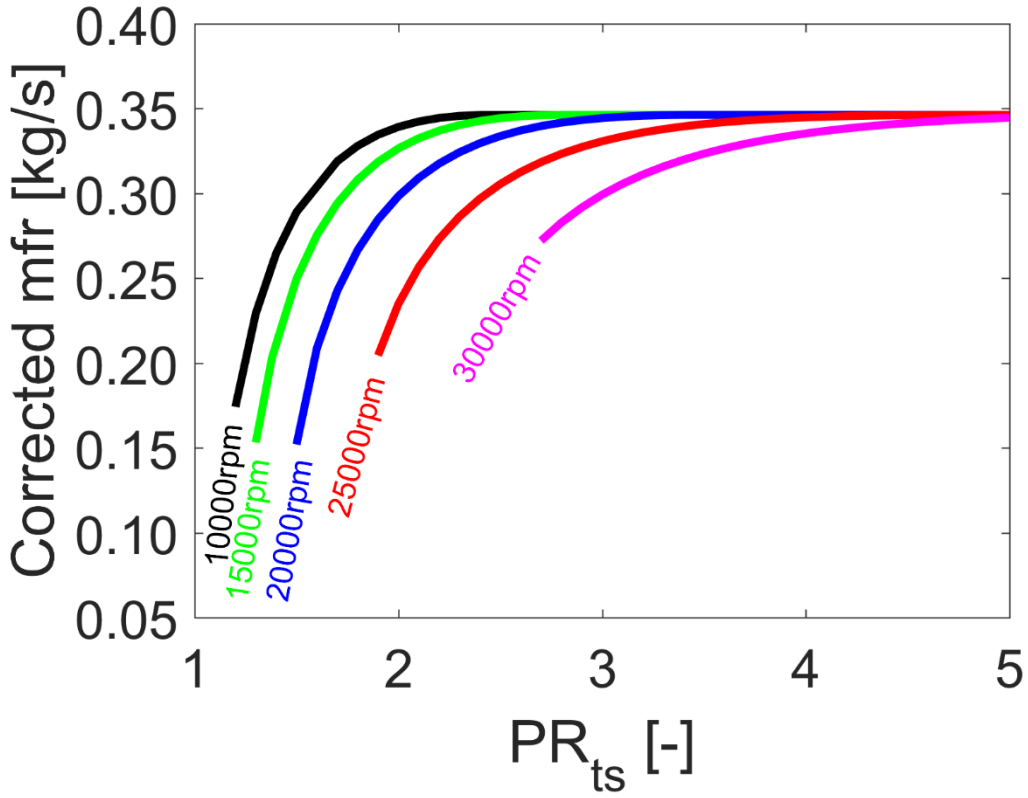

Figure 14: Prediction of corrected mass flowrate for Turbine A using R123.

5. Conclusion

This study presents the development, validation and application of a novel radial expander performance model. The predictions of the proposed model were compared with experimental data for both air and real gas under various rotational speeds, pressure ratios and mass flowrate conditions.

The accuracy of the proposed model when predicting the performance of an air turbine was tested. The error of the model lied between -2% and 9% for the prediction of the mass flowrate while the error on isentropic efficiency lied between -4% and 5%. The mean prediction error was found to be less than 5% for both mass flowrate and isentropic efficiency under all rotational speeds.

Then the model was validated against real gas turbine performance data (R123). The maximum error of the proposed model for both isentropic efficiency and expander power output was less than 6.5% for subsonic operating conditions. It has to be mentioned that as far as authors are aware, this is the first time that such an off-design model is validated against real gas data.

The utilization of the proposed model to develop performance maps for various organic fluids has been finally presented. The air turbine was simulated with R123 as working fluid and the performance maps were presented for the same turbine geometry. Utilizing the air turbine geometry with a real gas working fluid results a 12% drop on maximum isentropic efficiency while peak isentropic efficiency occurs at 70% lower rotational speed.

Overall, the proposed model can efficiently predict performance maps for radial turbines that operate either with air or with real gas fluids with high accuracy (within 10% error) and low computational cost. The latter makes this model a useful tool for the investigation of accurate transient simulations of organic Rankine cycles and the optimization of working fluids. The optimization of working fluids for ORC systems under transient conditions, with special focus on expanders, is part of the authors' future work.

Acknowledgements

The authors would like to acknowledge the financial support of Innovate UK to this project (ref. TS/M012220/1).

References

[1] Environmental Protection Agency (EPA), "U.s. greenhouse gas inventory report: 1990-2013. 2013.," 2013.

[2] Z. Samaras and I. Vouitsis, "3.13 - Transportation and Energy," Academic Press, Oxford, 2013.

[3] D. Zhu and X. Zheng, "Asymmetric twin-scroll turbocharging in diesel engines for energy and emission improvement," *Energy*, vol. 141, pp. 702–714, 2017.

[4] A. J. Feneley, A. Pesiridis, and A. M. Andwari, "Variable Geometry Turbocharger Technologies for Exhaust Energy Recovery and Boosting-A Review," *Renew. Sustain. Energy Rev.*, vol. 71, pp. 959–975, 2017.

[5] J. Cheong, S. Cho, and C. Kim, "Effect of Variable Geometry Turbocharger on HSDI Diesel Engine," in *Seoul 2000 FISITA World Automotive Congress*, 2000.

[6] M. S. Chiong, S. Rajoo, R. F. Martinez-Botas, and A. W. Costall, "Engine turbocharger performance prediction: One-dimensional modeling of a twin entry turbine," *Energy Convers. Manag.*, vol. 57, pp. 68–78, 2012.

[7] T. V Johnson, "Review of Vehicular Emissions Trends," *SAE Int. J. Engines. 8(3)1152-1167, 2015, doi 10.4271/2015-01-0993.*, 2015.

[8] C. Sprouse and C. Depcik, "Review of organic Rankine cycles for internal combustion engine exhaust waste heat recovery," *Appl. Therm. Eng.*, vol. 51, no. 1–2, pp. 711–722, 2013.

[9] A. B. Ma. Mohd, "Design and Development of a High Performance LPT for Electric Turbocompounding Energy Recovery Unit in a Heavily Downsized Engine," Ph.D Thesis, Imperial College London, 2012.

[10] X. Zhang, L. Wu, X. Wang, and G. Ju, "Comparative study of waste heat steam SRC, ORC and S-ORC power generation systems in medium-low temperature," *Appl. Therm. Eng.*, vol. 106, pp. 1427–1439, Aug. 2016.

[11] H. G. Zhang, E. H. Wang, and B. Y. Fan, "A performance analysis of a

novel system of a dual loop bottoming organic Rankine cycle (ORC) with a light-duty diesel engine," *Appl. Energy*, vol. 102, pp. 1504–1513, 2013.

[12] K. Yang *et al.*, "Performance Analysis of the Vehicle Diesel Engine-ORC Combined System Based on a Screw Expander," *Energies*, vol. 7, no. 5, pp. 3400–3419, 2014.

[13] A. Karvountzis-Kontakiotis *et al.*, "Effect of an ORC Waste Heat Recovery System on Diesel Engine Fuel Economy for Off-Highway Vehicles." SAE International , 2017.

[14] H. Schmid, "Less emissions through waste heat recovery," *Green Sh. Technol. Conf.*, no. April, 2004.

[15] K. K. Srinivasan, P. J. Mago, and S. R. Krishnan, "Analysis of exhaust waste heat recovery from a dual fuel low temperature combustion engine using an Organic Rankine Cycle," *Energy*, vol. 35, no. 6, pp. 2387–2399, Jun. 2010.

[16] K. Rahbar, S. Mahmoud, and R. K. Al-Dadah, "Mean-line modeling and CFD analysis of a miniature radial turbine for distributed power generation systems," *Int. J. Low-Carbon Technol.*, pp. 1–12, 2014.

[17] S. Quoilin, "Experimental study and modeling of a low temperature Rankine cycle for small scale cogeneration," Electro-Mechanical Engineer Thesis, University OF Liege, 2007.

[18] E. H. Wang, H. G. Zhang, B. Y. Fan, M. G. Ouyang, Y. Zhao, and Q. H. Mu, "Study of working fluid selection of organic Rankine cycle (ORC) for engine waste heat recovery," *Energy*, vol. 36, no. 5, pp. 3406–3418, 2011.

[19] D. Fiaschi, G. Manfrida, and F. Maraschiello, "Thermo-fluid dynamics preliminary design of turbo-expanders for ORC cycles," *Appl. Energy*, vol. 97, pp. 601–608, Sep. 2012.

[20] K. Darvish, A. M. Ehyaei, F. Atabi, and A. M. Rosen, "Selection of Optimum Working Fluid for Organic Rankine Cycles by Exergy and Exergy-Economic Analyses," *Sustainability* , vol. 7, no. 11. 2015.

[21] L. Pan and H. Wang, "Heat Recovery Systems: A Directory of Equipment and Techniques," *Appl. Therm. Eng.*, vol. 61, no. 2, pp. 606–615, 2013.

[22] Johnston J. R., “Evaluation of Expanders for Use in A Solar-Powered Rankine Cycle Heat Engine,” The Ohio State University, 2001.

[23] T. Wang, Y. Zhang, Z. Peng, and G. Shu, “A review of researches on thermal exhaust heat recovery with Rankine cycle,” *Renew. Sustain. Energy Rev.*, vol. 15, no. 6, pp. 2862–2871, 2011.

[24] J. Bao and L. Zhao, “A review of working fluid and expander selections for organic Rankine cycle,” *Renew. Sustain. Energy Rev.*, vol. 24, pp. 325–342, 2013.

[25] G. Qiu, H. Liu, and S. Riffat, “Expanders for micro-CHP systems with organic Rankine cycle,” *Appl. Therm. Eng.*, vol. 31, no. 16, pp. 3301–3307, 2011.

[26] R. Stobart and R. Weerasinghe, “Heat Recovery and Bottoming Cycles for SI and CI engines - A Perspective,” *SAE Techinical Pap. 2006-01-0662*, vol. 2006, no. 724, 2006.

[27] G. Latz, S. Andersson, and K. Munch, “Selecting an Expansion Machine for Vehicle Waste-Heat Recovery Systems Based on the Rankine Cycle,” *SAE Int.*, vol. 1, pp. 1–15, 2013.

[28] B. Saadatfar, R. Fakhrai, and T. Fransson, “Waste heat recovery Organic Rankine cycles in sustainable energy conversion: A state-of-the-art review,” *J. MacroTrends Energy Sustain.*, vol. 1, no. 1, pp. 161–188, 2013.

[29] H. Saravanamuttoo, G. Rogers, H. Cohen, and P. Straznicky, *Gas Turbine Theory*, 6th ed. Pearson Education Limited, 2009.

[30] ANDREA PALTRINIERI, “A MEAN-LINE MODEL TO PREDICT THE DESIGN PERFORMANCE OF RADIAL INFLOW TURBINES IN ORGANIC RANKINE CYCLES,” *Master Thesis*, 2014.

[31] E. Sauret and A. S. Rowlands, “Candidate radial-inflow turbines and high-density working fluids for geothermal power systems,” *Energy*, vol. 36, no. 7, pp. 4460–4467, 2011.

[32] F. Alshammari, A. Karvountzis-Kontakiotis, and A. Pesiridis, “Radial turbine expander design for organic rankine cycle, waste heat recovery in high efficiency, off-highway vehicles,” in *3rd Biennial International Conference on Powertrain Modelling and Control (PMC 2016), Loughborough, UK*, 2016.

[33] S. Quoilin, M. Van Den Broek, S. Declaye, P. Dewallef, and V. Lemort, "Techno-economic survey of Organic Rankine Cycle (ORC) systems," *Renew. Sustain. Energy Rev.*, vol. 22, pp. 168–186, 2013.

[34] J. Mowill and L.-U. Axelsson, "AXIAL AND RADIAL TURBINES: HOW DO THEY COMPARE IN THE 1-TO-3 MW POWER RANGE ?," *www.turbomachinerymag.com*, 2012. .

[35] B. F. Tchanche, G. Lambrinos, A. Frangoudakis, and G. Papadakis, "Low-grade heat conversion into power using organic Rankine cycles – A review of various applications," *Renew. Sustain. Energy Rev.*, vol. 15, no. 8, pp. 3963–3979, Oct. 2011.

[36] N. Yamada, T. Minami, and M. N. Anuar Mohamad, "Fundamental experiment of pumpless Rankine-type cycle for low-temperature heat recovery," *Energy*, vol. 36, no. 2, pp. 1010–1017, Feb. 2011.

[37] R. Capata and G. Hernandez, "Preliminary Design and Simulation of a Turbo Expander for Small Rated Power Organic Rankine Cycle (ORC)," *Energies*, vol. 7, no. 11, pp. 7067–7093, 2014.

[38] A. Pesiridis, B. Vassil, M. Padzillah, and R. Martinez-Botas, "A Comparison of flow control devices for variable geometry turbocharger application," *International Journal of Automotive Engineering and Technologies*, vol. 3. Murat CİNİVİZ, pp. 1–21, 2013.

[39] J. Walkingshaw, S. Spence, J. Ehrhard, and D. Thornhill, "An Experimental Assessment of the Effects of Stator Vane Tip Clearance Location and Back Swept Blading on an Automotive Variable Geometry Turbocharger," *J. Turbomach.*, vol. 136, no. 6, pp. 61001–61009, Nov. 2013.

[40] Z. Bo, Z. Sang, Q. Zhang, and Y. Weng, "Analysis of Radial Turbine of ORC Power Generation System for Low Temperature Heat Sources," no. 56604. p. V001T13A005, 2015.

[41] C. S. Wong, D. Meyer, and S. Krumdieck, "Selection and Conversion of Turbocharger As Turbo-Expander for Organic Rankine Cycle (Orc)," *35th New Zeakand Geotherm. Work.*, no. November, pp. 1–8, 2013.

[42] D.-Y. Kim and Y.-T. Kim, "Preliminary design and performance analysis of a radial inflow turbine for organic Rankine cycles," *Appl. Therm. Eng.*, vol.

120, pp. 549–559, Jun. 2017.

[43] C. S. K. Belloni, R. H. J. Willden, and G. T. Houlsby, “An investigation of ducted and open-centre tidal turbines employing CFD-embedded BEM,” *Renew. Energy*, vol. 108, pp. 622–634, Aug. 2017.

[44] A. M. Al Jubori, R. K. Al-Dadah, S. Mahmoud, and A. Daabo, “Modelling and parametric analysis of small-scale axial and radial-outflow turbines for Organic Rankine Cycle applications,” *Appl. Energy*, vol. 190, pp. 981–996, Mar. 2017.

[45] L. Barr, S. W. T. Spence, and P. Eynon, “Improved Performance of a Radial Turbine Through the Implementation of Back Swept Blading,” no. 43161. pp. 1459–1468, 2008.

[46] S. Kim, J. Park, and J. Baek, “A numerical study of the effects of blade angle distribution on the performance and loss generation of centrifugal compressor impellers,” *Proc. Inst. Mech. Eng. Part A J. Power Energy*, vol. 226, no. 2, pp. 208–217, Dec. 2011.

[47] A. M. Al Jubori, R. Al-Dadah, and S. Mahmoud, “An innovative small-scale two-stage axial turbine for low-temperature organic Rankine cycle,” *Energy Convers. Manag.*, vol. 144, no. Supplement C, pp. 18–33, 2017.

[48] A. Kasaeian, A. R. Mahmoudi, F. R. Astaraei, and A. Hejab, “3D simulation of solar chimney power plant considering turbine blades,” *Energy Convers. Manag.*, vol. 147, no. Supplement C, pp. 55–65, 2017.

[49] A. Al Jubori, A. Daabo, R. K. Al-Dadah, S. Mahmoud, and A. B. Ennil, “Development of micro-scale axial and radial turbines for low-temperature heat source driven organic Rankine cycle,” *Energy Convers. Manag.*, vol. 130, no. Supplement C, pp. 141–155, 2016.

[50] A. M. Daabo, A. Al Jubori, S. Mahmoud, and R. K. Al-Dadah, “Parametric study of efficient small-scale axial and radial turbines for solar powered Brayton cycle application,” *Energy Convers. Manag.*, vol. 128, no. Supplement C, pp. 343–360, 2016.

[51] J. R. Serrano, F. J. Arnau, L. M. García-Cuevas, A. Dombrovsky, and H. Tartoussi, “Development and validation of a radial turbine efficiency and mass flow model at design and off-design conditions,” *Energy Convers. Manag.*, vol. 128, no. Supplement C, pp. 281–293, 2016.

[52] A. Al Jubori, R. K. Al-Dadah, S. Mahmoud, A. S. B. Ennil, and K. Rahbar, "Three dimensional optimization of small-scale axial turbine for low temperature heat source driven organic Rankine cycle," *Energy Convers. Manag.*, vol. 133, no. Supplement C, pp. 411–426, 2017.

[53] D. Hu, S. Li, Y. Zheng, J. Wang, and Y. Dai, "Preliminary design and off-design performance analysis of an Organic Rankine Cycle for geothermal sources," *Energy Convers. Manag.*, vol. 96, no. Supplement C, pp. 175–187, 2015.

[54] F. Alshammari, A. Karvountzis-Kontakiotis, A. Pesiridis, and T. Minton, "Radial Expander Design for an Engine Organic Rankine Cycle Waste Heat Recovery System," *Energy Procedia*, vol. 129, pp. 285–292, Sep. 2017.

[55] R. N. Pinto, A. Afzal, L. V. D'Souza, Z. Ansari, and A. D. Mohammed Samee, "Computational Fluid Dynamics in Turbomachinery: A Review of State of the Art," *Arch. Comput. Methods Eng.*, pp. 1–13, 2016.

[56] F. A. Muggli, P. Holbein, and P. Dupont, "CFD Calculation of a Mixed Flow Pump Characteristic From Shutoff to Maximum Flow," *J. Fluids Eng.*, vol. 124, no. 3, pp. 798–802, Aug. 2002.

[57] W. Jansen and E. B. Qvale, "A Rapid Method for Predicting the Off-Design Performance of Radial-Inflow Turbines," *ASME -PUBLICATIONS-*, no. 80067, p. V001T01A002, 1967.

[58] A. Dadone and M. Pandolfi, "A method for evaluating the off-design performance of a radial inflow turbine and comparison with experiments," *Int. J. Mech. Sci.*, vol. 11, no. 3, pp. 241–252, 1969.

[59] C. A. Wasserbauer and A. J. Glassman, "Fortran Program for Predicting Off-Design Performance of Radial-Inflow Turbines," National Aeronautics and Space Administration, Washington, D.C, 1975.

[60] P. L. Meitner and A. J. Glassman, "Off-design performance loss model for radial turbines with pivoting, variable-area stators," NASA Lewis Research Center; Propulsion Lab, Cleveland, OH, United States, 1980.

[61] A. Whitfield and N. C. Baines, *Design of Radial Turbomachines*. Longman Scientific and Technical, Harlow, England, 1990.

[62] S. K. Ghosh, "Experimental and Computational Studies on Cryogenic

Turboexpander," PhD thesis. National Institute of Technology, 2008.

[63] L. J. Kastner and F. S. Bhinder, "A Method for Predicting the Performance of a Centripetal Gas Turbine Fitted With a Nozzle-Less Volute Casing," no. 79771. p. V01BT02A003, 1975.

[64] N. C. Baines, "A Meanline Prediction Method for Radial Turbine Efficiency," in *6th International Conference on Turbocharging and Air Management Systems, IMechE Conference Transactions, C554/008/98*.

[65] "NextORC: Fundamental studies on Organic Rankine Cycle expanders." [Online]. Available: https://www.city.ac.uk/mathematics-computer-science-engineering/research/thermo-fluids/nextorc.

[66] H. Moustapha, M. F. Zelesky, N. C. Baines, and D. Japikse, *Axial and Radial Turbines*, 1st ed. White River Junction: Concepts NREC, 2003.

[67] N. C. Baines, "Radial Turbines, an integrated design approach," in *6th European conference on Turbomachinery- Fluid Dynamics and Thermodynamics.*, 2005.

[68] R. S. Benson, "An Analysis of the Losses in a Radial Gas Turbine," *Proc. Inst. Mech. Eng. Conf. Proc.*, vol. 180, no. 10, pp. 41–53, Jun. 1965.

[69] G. F. Hiett and I. H. Johnston, "Experiments Concerning the Aerodynamic Performance of Inward Flow Radial Turbines," *Proc. Inst. Mech. Eng. Conf. Proc.*, vol. 178, no. 9, pp. 28–42, Jun. 1963.

[70] R. S. Benson, W. G. Cartwright, and S. K. Das, "An Investigation of the Losses in the Rotor of a Radial Flow Gas Turbine at Zero Incidence under Conditions of Steady Flow," *Proc. Inst. Mech. Eng. Conf. Proc.*, vol. 182, no. 8, pp. 221–231, Sep. 1967.

[71] C. Rodgers, "Small High Pressure Ratio Radial Turbine Technology," *VKI Lect. Ser.*, 1987.

[72] O. Balje, "Contribution to the Problem of Designing Radial Turbomachines," *Trans ASME 741451*, 1952.

[73] S. W. Churchill, "Empirical Expressions for the Shear Stressing Turbulent Flow in Commercial Pipe," *AIChE J.*, vol. 19, no. 2, pp. 375–376, 1973.

[74] S. . Churchill, “Friction-factor Equation Spans all Fluid Flow Regimes,” *Chem. Eng. (New York) 84 (24), pp. 91–92*, 1977.

[75] R. H. Aungier, *Turbine aerodynamics: Axial-flow and radial-inflow turbine design and analysis*, 1st ed. New York, 2006.

[76] M. White, “The design and analysis of radial inflow turbines implemented within low temperature organic Rankine cycles,” PhD thesis. City University London, 2015.

[77] S. Li, E. M. Krivitzky, and X. Qiu, “Meanline Modeling of a Radial-Inflow Turbine Nozzle With Supersonic Expansion,” no. 49729. p. V02DT42A036, 2016.

[78] R. S. Benson, “A review of methods for assessing loss coefficients in radial gas turbines,” *Int. J. Mech. Sci.*, vol. 12, no. 10, pp. 905–932, 1970.

[79] J. D. Stanitz, “Some Theoretical Aerodynamic Investigations of Impellers in Radial-and Mixed-Flow Centrifugal Compressors,” *ASME Trans.*, vol. 74, pp. 473–497, 1952.

[80] S. L. Dixon and C. Hall, *Fluid Mechanics and Thermodynamics of Turbomachinery*. Butterworth-Heinemann: Burlington, 2010.

[81] P. He, Z. Sun, B. Guo, H. Chen, and C. Tan, “Aerothermal Investigation of Backface Clearance Flow in Deeply Scalloped Radial Turbines,” *J. Turbomach.*, vol. 135, no. 2, pp. 21002–21012, Oct. 2012.

[82] J. W. Daily and R. E. Nece, “Chamber Dimension Effects on Induced Flow and Frictional Resistance of Enclosed Rotating Disks,” *J. Basic Eng.*, vol. 82, no. 1, pp. 217–230, Mar. 1960.

[83] J. F. Suhrmann, D. Peitsch, M. Gugau, T. Heuer, and U. Tomm, “Validation and Development of Loss Models for Small Size Radial Turbines,” no. 44021. pp. 1937–1949, 2010.

[84] S. W. T. Spence, W. J. Doran, and D. W. Artt, “Experimental performance evaluation of a 99.0 mm radial inflow nozzled turbine at larger stator-rotor throat area ratios,” *Proc. Inst. Mech. Eng. Part A J. Power Energy*, vol. 213, no. 3, pp. 205–218, May 1999.

[85] L. Shao, J. Zhu, X. Meng, X. Wei, and X. Ma, “Experimental study of an organic Rankine cycle system with radial inflow turbine and R123,” *Appl. Therm. Eng.*, vol. 124, no. Supplement C, pp. 940–947, 2017.

[86] O. Redlich and J. Kwong, “On the Thermodynamics of Solutions. V. An Equation of State. Fugacities of Gaseous Solutions.,” *Chem. Rev.*, vol. 44, no. 1, pp. 233–244, 1949.

[87] G. Soave, “Equilibrium constants from a modified Redlich-Kwong equation of state,” *Chem. Eng. Sci.*, vol. 27, no. 6, pp. 1197–1203, 1972.

[88] D.-Y. Peng and D. B. Robinson, “A New Two-Constant Equation of State,” *Ind. Eng. Chem. Fundam.*, vol. 15, no. 1, pp. 59–64, 1976.

[89] E. Lemmon, M. Huber, and M. McLinden, “NIST Standard Reference Database 23: Reference Fluid Thermodynamic and Transport Properties-REFPROP, Version 9.0, National Institute of Standards and Technology, Standard Reference Data Program, Gaithersburg, Maryland, USA.” 2010.

[90] N. Sakellaridis and D. Hountalas, “Meanline Modeling of Radial Turbine Performance for Turbocharger Simulation and Diagnostic Applications,” in *SAE 2013 World Congress & Exhibition*, 2013.

[91] M. White and A. I. Sayma, “The Application of Similitude Theory for the Performance Prediction of Radial Turbines Within Small-Scale Low-Temperature Organic Rankine Cycles,” *J. Eng. Gas Turbines Power*, vol. 137, no. 12, pp. 122605–122610, Jul. 2015.